Supporting Information

Multiphase Chemistry of Glyoxal: Revised Kinetics of the Alkyl Radical Reaction with Molecular Oxygen and the Reaction of Glyoxal with OH, NO_3 and SO_4^- in Aqueous Solution

Prepared for Environmental Science & Technology

T. Schaefer, D. van Pinxteren and H. Herrmann*

Leibniz-Institute for Tropospheric Research (TROPOS), Atmospheric Chemistry Department, Permoserstraße 15, 04318 Leipzig, Germany

* Corresponding author phone: +49 341 2717 7024; fax: +49 341 2717 99 7024; e-mail: herrmann@tropos.de

Number of Pages: 30

Number of Tables: 4

Table Captions

Table SI 1: Change of the initial concentration of OH radicals and the photolysis fragments concentration of the ferricyanide complex with $[H_2O_2] = 5 \times 10^{-3}$ M and [Reactant] $= 1 \times 10^{-3}$ M

Table SI 2: Full reaction mechanism with rate constants used to simulate the experiments with $[H_2O_2] = 2 \times 10^{-4}$ M and [Glyoxal] $= 1 \times 10^{-3}$ M at pH = 2.

Table SI 3: Influence of the change of the molar absorption coefficient of the glycolic acid alkyl ε(R') and peroxyl radical ε(R'O_2) on the oxygen addition reaction of glyoxyl alkyl radical ε(R) to the glyoxyl peroxyl radical ε(RO_2) at λ = 244nm.

Table SI 4: Temperature dependent second-order rate constants for the OH, SO_4^- and NO_3 radical reaction with glyoxal.

Number of Figures: 23

Figure Captions

Figure SI 1: Intercomparison of the spectra of ferricyanide ($K_3[Fe(CN)_6]$) and ferrocyanide ($K_4[Fe(CN)_6]$) in neutral solution.

Figure SI 2: Measured absorption - time profiles at $\lambda = 442$ nm for the bleaching reaction of ferricyanide due to the α-alkyl radicals form in the reaction of OH radicals with methanol.

Figure SI 3: The averaged first-order rate constants (left axis) for five different ferricyanide concentrations plotted against these concentrations. At the right axis the measured oxygen concentration is given.

Figure SI 4: Measured absorption - time profiles at $\lambda = 442$ nm of the reaction from the formed ferrocyanide with H_2O_2 in the investigation of the methanol oxidation.

Figure SI 5: Absorbance change for the different solutions, with the concentrations with $[H_2O_2] = 5 \times 10^{-3}$ M, [Methanol] = 1×10^{-3} M, $[K_3[Fe(CN)_6]] = 5 \times 10^{-5}$ M and a various O_2 content.

Figure SI 6: Absorbance ratio A_0/A_X from the reaction with methanol plotted against $[O_2]/[Fe(CN)_6]^{3-}$ with a linear force through one. On the right axis the measured oxygen concentration is given.

Figure SI 7: Measured absorption - time profiles at $\lambda = 442$ nm for the bleaching reaction of ferricyanide due to the α-alkyl radicals form in the reaction of OH radicals with 2-propanol.

Figure SI 8: The averaged first-order rate constants (left axis) for five different ferricyanide concentrations plotted against these concentrations. At the right axis the measured oxygen concentration is given.

Figure SI 9: Measured absorption - time profiles at $\lambda = 442$ nm of the reaction from the formed ferrocyanide with H_2O_2 in the investigation of the 2-propanol

Figure SI 10: Absorbance change for the different solutions, with the concentrations with $[H_2O_2] = 5 \times 10^{-3}$ M, [2-propanol] = 1×10^{-3} M, $[K_3[Fe(CN)_6]] = 5 \times 10^{-5}$ M and a various O_2 content.

Figure SI 11: Absorbance ratio A_0/A_X from the reaction with 2-propanol plotted against $[O_2]/[Fe(CN)_6]^{3-}$ with a linear force through one. On the right axis the measured oxygen concentration is given.

Figure SI 12: Measured absorption - time profiles at λ = 442 nm of the photolysis of $[K_3[Fe(CN)_6]] = 5 \times 10^{-5}$ M (red) and $[K_3[Fe(CN)_6]] = 5 \times 10^{-5}$ M with $[H_2O_2] = 5 \times 10^{-3}$ M (green).

Figure SI 13: Measured absorption - time profiles at λ = 420 nm of the oxidation reaction of ferrocyanide with H_2O_2 at pH = 2 to form the absorbing ferricyanide.

Figure SI 14: The averaged first-order rate constants of the decay of ferrocyanide with H_2O_2 at pH = 2 plotted against the ferrocyanide concentrations.

Figure SI 15: The averaged first-order rate constants of the reaction with the glyoxyl alkyl radical (left axis) for five different ferricyanide concentrations plotted against these concentrations. At the right axis the measured oxygen concentration is given.

Figure SI 16: Measured absorption - time profiles at λ = 442 nm of the reaction from the formed ferrocyanide with H_2O_2 in the investigation of the glyoxal oxidation.

Figure SI 17: Measured - time profiles at λ = 244 nm of the glyoxal oxidation in oxygen reduced solution. The modelling provided the first order rate constant of the acid-catalyzed dehydration reaction.

Figure SI 18: Measured and modelled absorption - time profiles at λ = 244 nm of the decay of HO_2, glyoxyl peroxyl and glycolic acid peroxyl radical in an oxygen saturated solution.

Figure SI 19: Classical method ln c vs. t for the determination of k_{1st} derived from absorption - time profiles at λ = 244 nm of an oxygen saturated solution.

Figure SI 20: Absorbance change for the different solutions, with the concentrations with $[H_2O_2] = 5 \times 10^{-3}$ M, [Glyoxal] = 1×10^{-3} M, $[K_3[Fe(CN)_6]] = 5 \times 10^{-5}$ M and at various pH values.

Figure SI 21: Arrhenius plot for the reaction of OH radicals with glyoxal in aqueous solution.

Figure SI 22: Arrhenius plot for the reaction of sulphate radicals with glyoxal in aqueous solution.

Figure SI 23: Arrhenius plot for the reaction of nitrate radicals with glyoxal in aqueous solution.

Reagents and Materials. The following chemicals were used as received: glyoxal (40% in water, Sigma-Aldrich), glyoxal trimer (≥98 %, Fluka), hydrogen peroxide (≥ 30% in water, Fluka), $NaNO_3$ (99.5 %, Riedel-de Haën), $K_2S_2O_8$ (≥ 99.0 %, Fluka), H_2O_2 (≥ 30 %, Fluka), KSCN (≥ 99.0 %, Fluka), $HClO_4$ (70 – 72 %, J. T. Baker Analyzed), $K_3[Fe(CN)_6]$ (99.0 %, Sigma-Aldrich), $K_4[Fe(CN)_6]$ x 3 H_2O (≥ 99.5 %, Fluka), oxygen gas (UltraPure, Air Products), argon gas (Premium, Air Products), catalase (from Coryne-bacterium glutamicum, ≥500000 U/mL in water, Sigma-Aldrich), tris(hydroxylmethyl)-aminomethane (≥ 99.9 %, Sigma-Aldrich), hexadimethrine bromide(≥ 95.0 %, Sigma-Aldrich) and 5 sulfosalicylic acid (for electrophoresis, Sigma Aldrich). All solutions were freshly prepared using Milli-Q grade water (18 MΩ cm, Millipore, Billerica, MA).

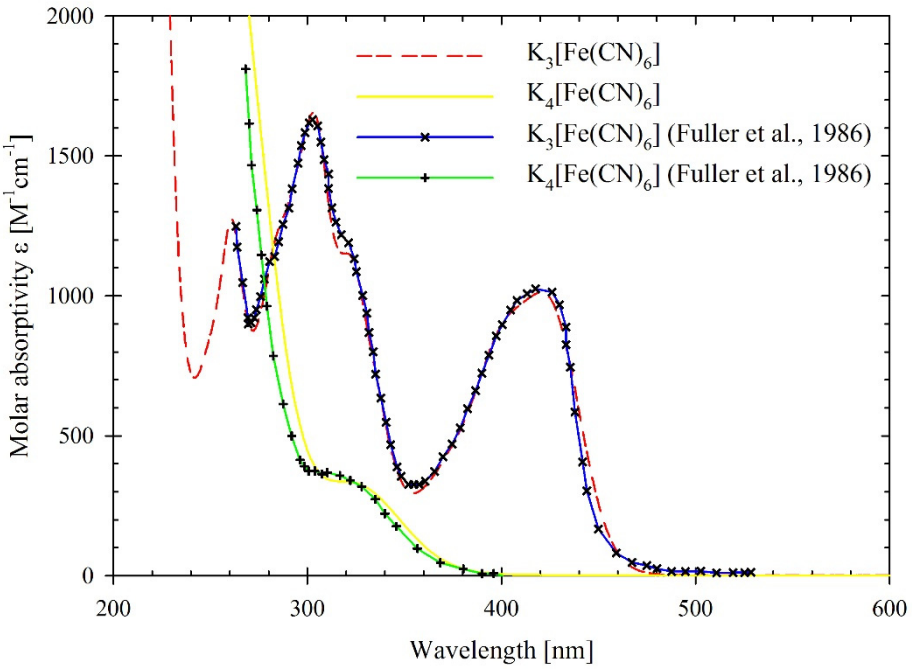

Figure SI 1: Intercomparison of the spectra of ferricyanide ($K_3[Fe(CN)_6]$) and ferrocyanide ($K_4[Fe(CN)_6]$) in neutral solution.[1]

Test of the Method from Adams et al. with the organic reactant methanol and 2-propanol.[2]

Methanol:

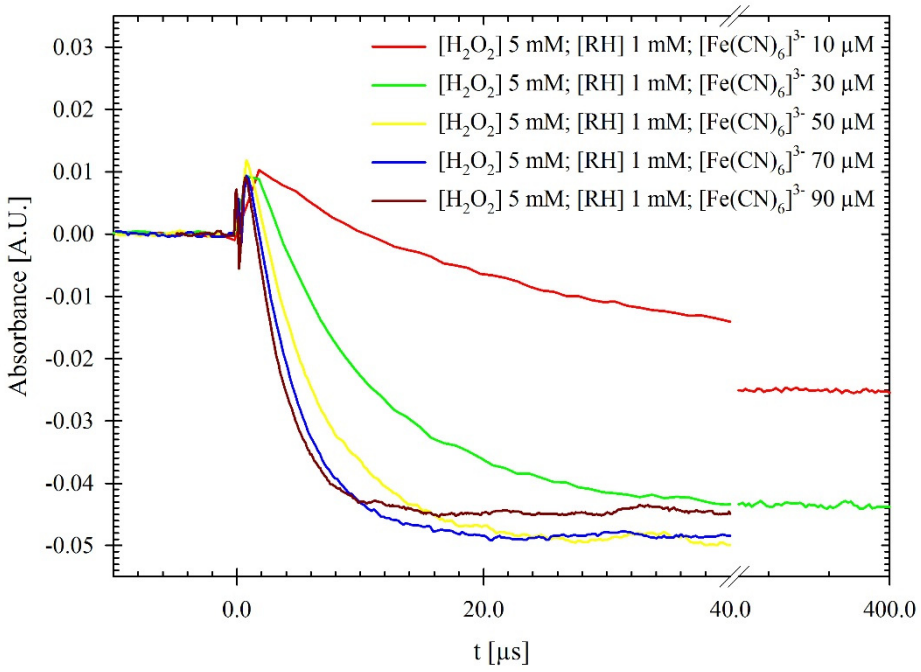

Figure SI 2: Measured absorption - time profiles at λ = 442 nm for the bleaching reaction of ferricyanide due to the α-alkyl radicals form in the reaction of OH radicals with methanol.

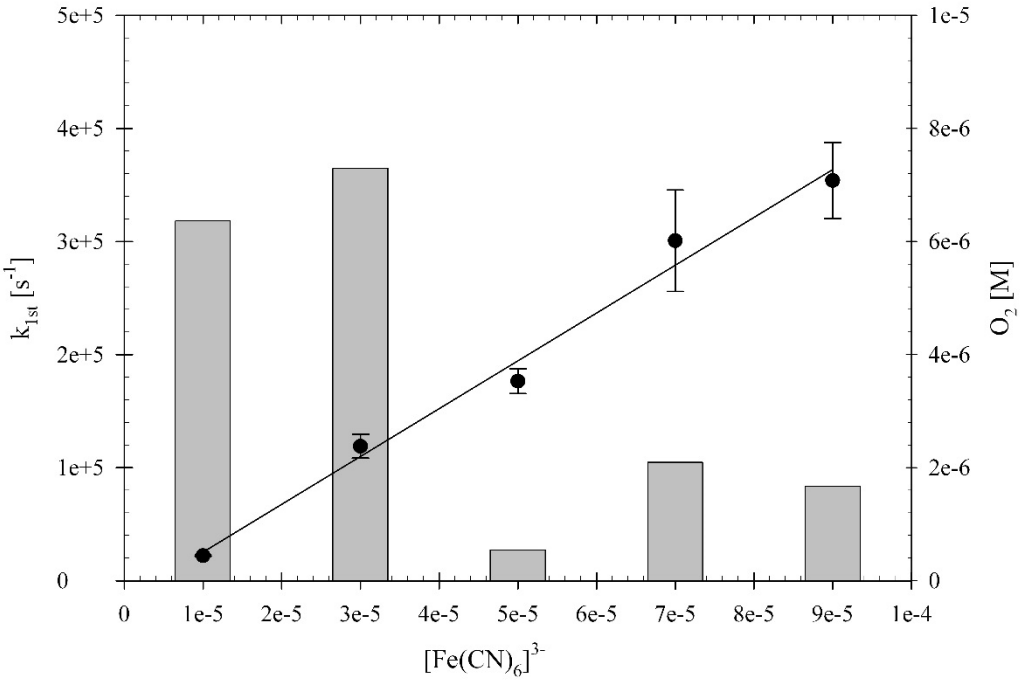

Figure SI 3: The averaged first-order rate constants (left axis) for five different ferricyanide concentrations plotted against these concentrations. At the right axis the measured oxygen concentration is given.

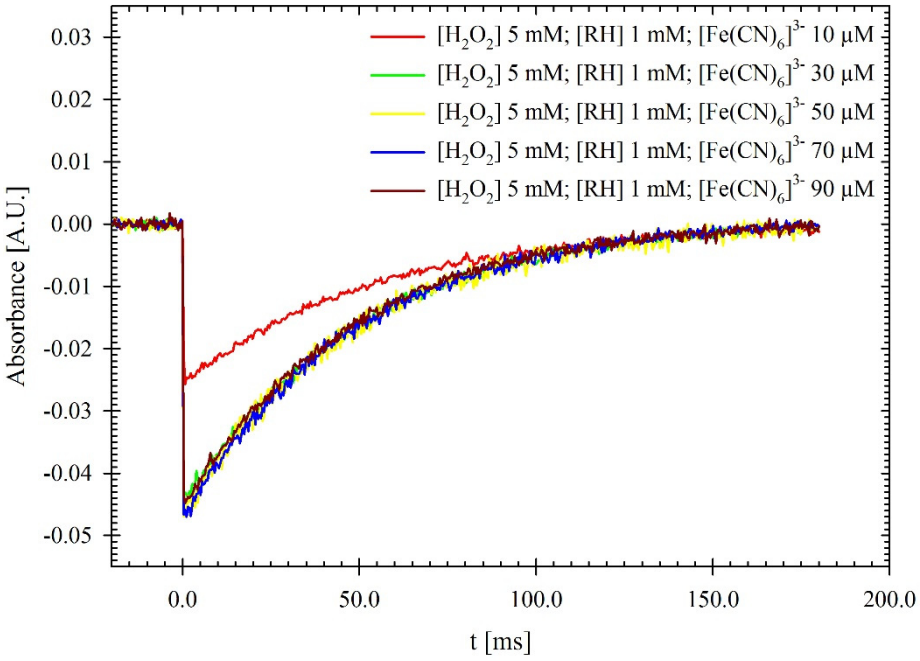

Figure SI 4: Measured absorption - time profiles at λ = 442 nm of the reaction from the formed ferrocyanide with H_2O_2 in the investigation of the methanol oxidation.

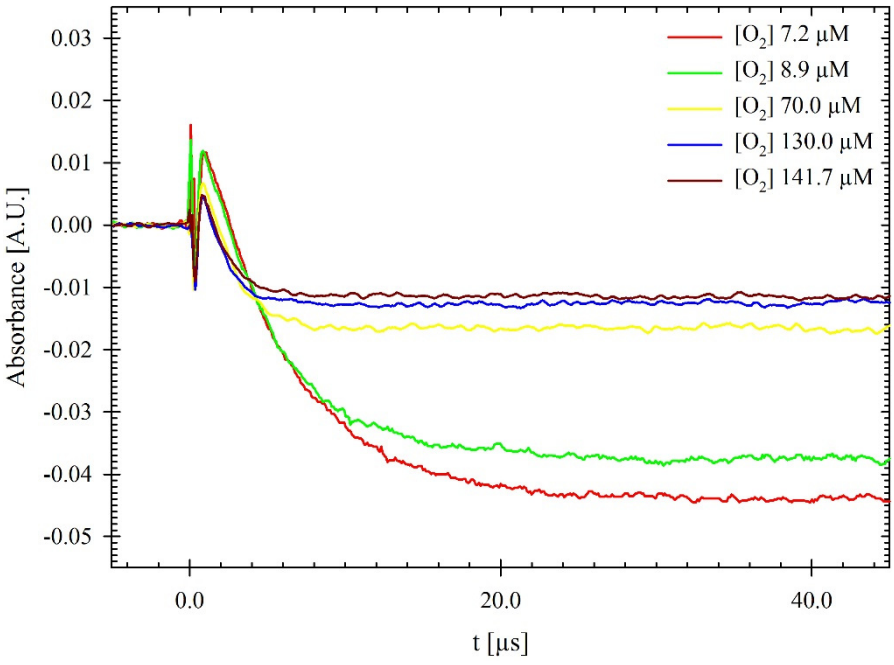

Figure SI 5: Absorbance change for the different solutions, with the concentrations with $[H_2O_2] = 5 \times 10^{-3}$ M, [Methanol] = 1×10^{-3} M, $[K_3[Fe(CN)_6]] = 5 \times 10^{-5}$ M and a various O_2 content.

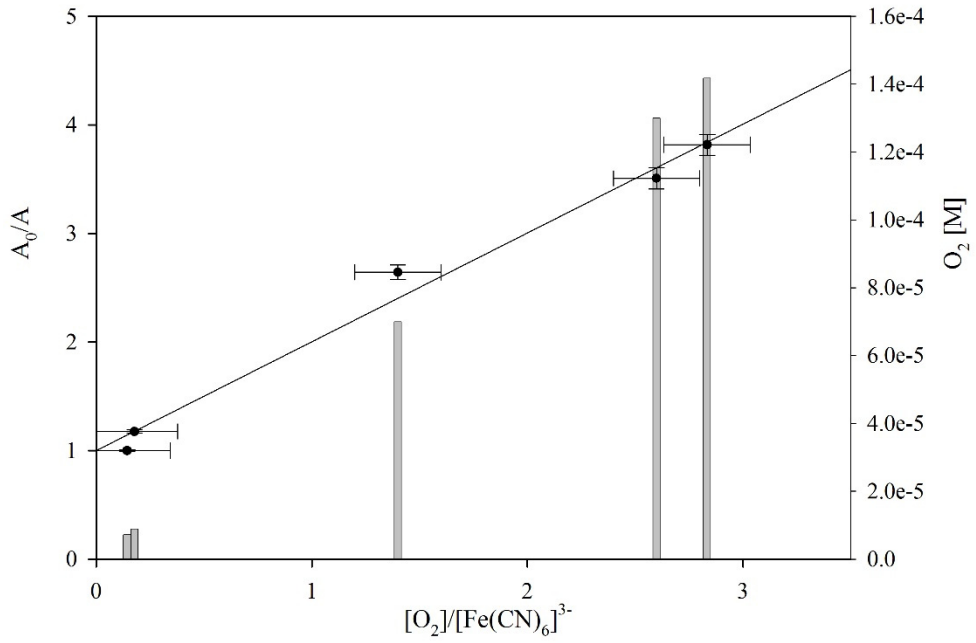

Figure SI 6: Absorbance ratio A_0/A_X from the reaction with methanol plotted against $[O_2]/[Fe(CN)_6]^{3-}$ with a linear force through one. On the right axis the measured oxygen concentration is given.

2-Propanol:

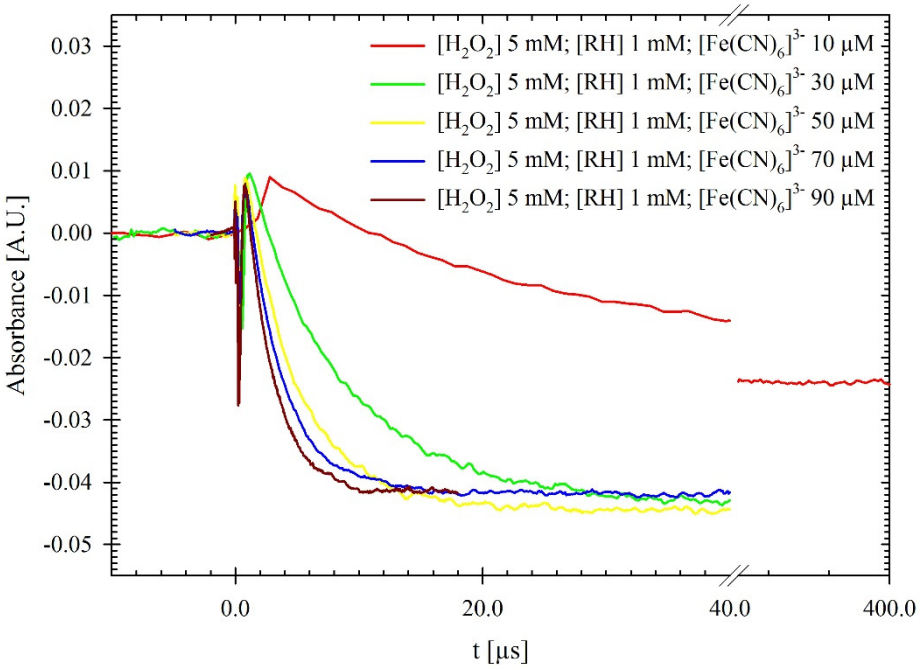

Figure SI 7: Measured absorption - time profiles at λ = 442 nm for the bleaching reaction of ferricyanide due to the α-alkyl radicals form in the reaction of OH radicals with 2-propanol.

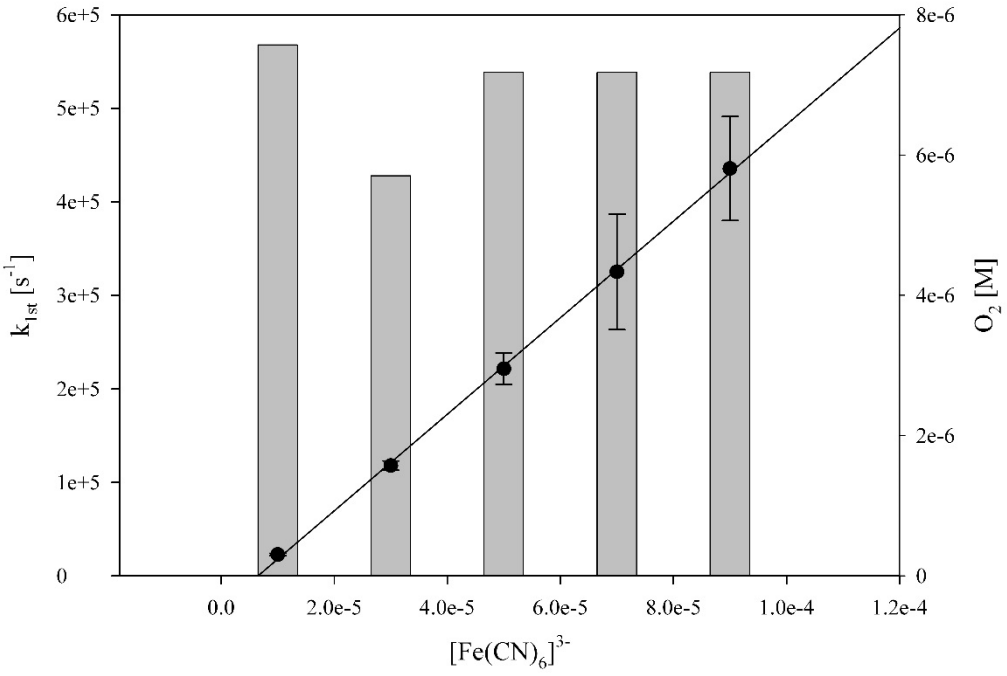

Figure SI 8: The averaged first-order rate constants (left axis) for five different ferricyanide concentrations plotted against these concentrations. At the right axis the measured oxygen concentration is given.

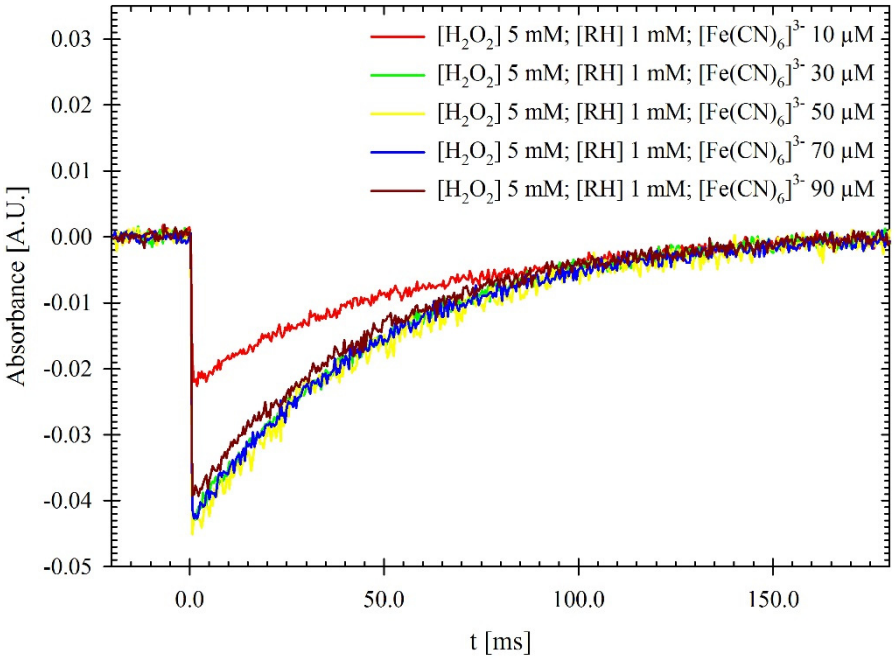

Figure SI 9: Measured absorption - time profiles at λ = 442 nm of the reaction from the formed ferrocyanide with H_2O_2 in the investigation of the 2-propanol oxidation.

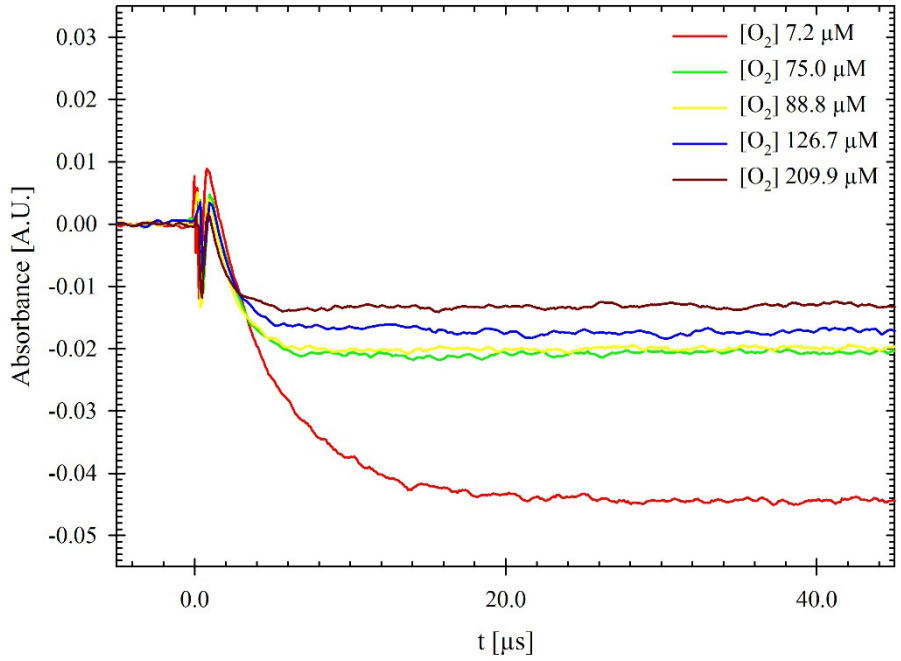

Figure SI 10: Absorbance change for the different solutions, with the concentrations with $[H_2O_2] = 5 \times 10^{-3}$ M, [2-propanol] = 1×10^{-3} M, $[K_3[Fe(CN)_6]] = 5 \times 10^{-5}$ M and a various O_2 content.

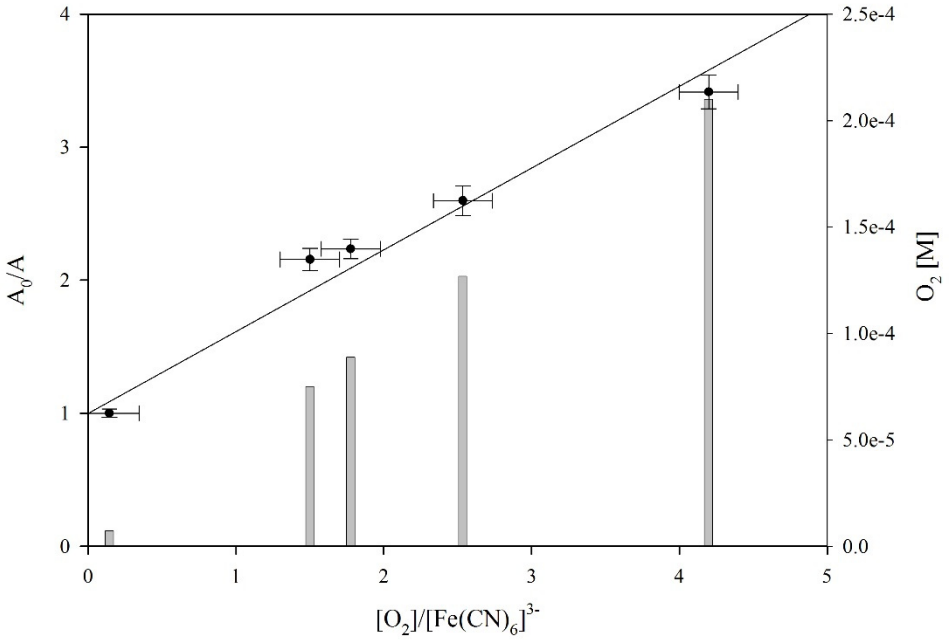

Figure SI 11: Absorbance ratio A_0/A_X from the reaction with 2-propanol plotted against $[O_2]/[Fe(CN)_6]^{3-}$ with a linear force through one. On the right axis the measured oxygen concentration is given.

Calculation of k_{1st} for the determination of $k(R + [Fe(CN)_6]^{3-})$

The slope of the measured inverted absorption - time profiles correspond to the following first order rate law:

$$\frac{d[A]}{dt} = -k_{1st}[A]$$

In combination with the Lambert Beer Law:

$$\text{Absorbance} = \log_{10}\left(\frac{I_0}{I}\right) = c \cdot \varepsilon \cdot d$$

The following expression can be obtained:

$$\ln\left(\frac{\log\left(\frac{I_0}{I_{t=0}}\right)(\varepsilon \cdot d)^{-1}}{\log\left(\frac{I_0}{I_t}\right)(\varepsilon \cdot d)^{-1}}\right) = -k_{1st}t$$

The initial OH radical concentration $[OH]_0$ is equal to the maximum alkyl radical concentration $[R]_{MAX,}$ therefore the initial intensity $I_{t=0}$ is equal to the maximum intensity I_{MAX}:

$$\ln\left(\frac{\log\left(\frac{I_0}{I_{MAX}}\right)(\varepsilon \cdot d)^{-1}}{\log\left(\frac{I_0}{I_t}\right)(\varepsilon \cdot d)^{-1}}\right) = -k_{1st}t$$

And simplified to:

$$\ln\ (I_t - I_{MAX}) = k_{1st}t$$

Whereas I_t is the light intensity at a defined time point after the laser pulse and I_{max} is the maximum light intensity.

Principles of the competition kinetics

The competition kinetic method based on the competition of two parallel running radical reactions (R-1) and (R-2).

$$[R\cdot] + [[Fe(CN)]^{3-}] \xrightarrow{k_1} [R'] + [[Fe(CN)]^{4-}] \qquad \text{(R-1)}$$

$$[R\cdot] + [O_2] \xrightarrow{k_2} [RO_2] \qquad \text{(R-2)}$$

In this case, the first reaction (R-1) corresponds to the alkyl radical [R·] reaction with the reference system ferricyanide [$K_3[Fe(CN)_6]$]. The second reaction (R-2) corresponds to the reaction of the alkyl radical [R·] with molecular oxygen [O_2]. The formation of the ferrocyanide [$K_4[Fe(CN)_6]$] as non-absorbing species at $\lambda = 442$ nm, leads to an observable bleaching of the solution. The presence of molecular oxygen reduced the yield of ferrocyanide. Both of these reaction follow a second order rate law (E-1) and (E-2).

$$\frac{d[R\cdot]}{dt} = -k_1 \times [R\cdot] \times [[Fe(CN)_6]^{3-}] \qquad \text{(E-1)}$$

$$\frac{d[R\cdot]}{dt} = -k_2 \times [R\cdot] \times [O_2] \qquad \text{(E-2)}$$

The decrease or change over the time of the alkyl radical concentration can described as follows:

$$-\frac{d[R\cdot]}{dt} = k_1 \times [R\cdot] \times [[Fe(CN)_6]^{3-}] + k_2 \times [R\cdot] \times [O_2] \qquad \text{(E-3)}$$

This equation (E-3) can be described under pseudo-first order condition of the two reactants ferricyanide and molecular oxygen compared to the alkyl radical as follows:

$$-\frac{d[R\cdot]}{dt} = k' \times [R\cdot] \qquad \text{with } k' = k_1 \times [[Fe(CN)_6]^{3-}] + k_2 \times [O_2] \qquad \text{(E-4)}$$

The branching ratio f of the parallel reactions (R-1) and (R-2) can be described by equation (E-5) and (E-6).[3]

$$f([Fe(CN)_6]^{4-}) = \frac{k_1 \times [[Fe(CN)_6]^{3-}]}{k'} = \frac{k_1 \times [[Fe(CN)_6]^{3-}]}{k_1 \times [[Fe(CN)_6]^{3-}] + k_2 \times [O_2]} \quad \text{(E-5)}$$

$$f([Fe(CN)_6]^{4-}) = \frac{[[Fe(CN)_6]^{4-}]}{[R\cdot]_0} \quad \text{(E-6)}$$

By equating the equations (E-5) and (E-6) the following expression can be obtained:

$$\frac{[[Fe(CN)_6]^{4-}]}{[R\cdot]_0} = \frac{k_1 \times [[Fe(CN)_6]^{3-}]}{k_1 \times [[Fe(CN)_6]^{3-}] + k_2 \times [O_2]} \quad \text{(E-7)}$$

or

$$\frac{[R\cdot]_0}{[[Fe(CN)_6]^{4-}]} = 1 + \frac{k_2 \times [O_2]}{k_1 \times [[Fe(CN)_6]^{3-}]} \quad \text{(E-8)}$$

The full conversion of the alkyl radical $[R]_0$ to ferrocyanide $[K_4[Fe(CN)_6]]_0$ is obtained, if no molecular oxygen is present.

$$\frac{[[Fe(CN)_6]^{4-}]_0}{[[Fe(CN)_6]^{4-}]} = 1 + \frac{k_2 \times [O_2]}{k_1 \times [[Fe(CN)_6]^{3-}]} \quad \text{(E-9)}$$

Instead of the concentration ratios in equation (G-2.11), the ratio of the absorbance's can be used. Due to the Lambert-Beer's law the ratio of the absorbance A at $\lambda = 442$ nm proportional to the ratio of the concentration of ferrocyanide $[K_4[Fe(CN)_6]]$. The following expression (E-10) can be obtained:

$$\frac{A_0}{A_x} = 1 + \frac{k_2 \times [O_2]}{k_1 \times [[Fe(CN)_6]^{3-}]} \quad \text{(E-10)}$$

Since it is known that the OH radicals, HO_x radicals, the alkyl radicals as well as the peroxyl radical do not absorb at $\lambda = 442$ nm no interference is expected from these transient species.

Determination of the photolysis laser energy

The average laser energy per pulse inside the measurement cell E = 177 mJ has been determined by using the persulfate photolysis with the detection of the formed SO_4^- radical. The following parameters were used for the calculations: $\varepsilon(SO_4^-)_{442\ nm}$ = 1600 M^{-1} cm^{-1}, $[SO_4^-]_0$ = 2.3 × 10^{-6} M, $\Phi_{248\ nm}(S_2O_8^{2-})$ = 1.6, $\varepsilon_{248\ nm}(S_2O_8^{2-})$ = 28.95 M^{-1} cm^{-1} and $[S_2O_8^{2-}]$ = 5 × 10^{-4} M.[4,5]

Contribution of the ferricyanide photolysis

The photolysis of ferricyanide has been described by Fuller et al. and leads to aquapentacyanoferrate(III) and cyanide in acidic and unbuffered aqueous solution. The quantum yield was given as Φ = 0.02 – 0.04.[1] The molar absorption coefficient of ferricyanide can be given with $\varepsilon_{248\ nm}$ = 810 M^{-1} cm^{-1} (Figure SI 1). Due to the light absorption of H_2O_2 ($c(H_2O_2)$ = 5 × 10^{-3} M) with molar absorption coefficient $\varepsilon_{248\ nm}$ = 25 M^{-1} cm^{-1} the direct photolysis of ferricyanide at λ = 248 nm was reduced (Figure SI 12). In this case H_2O_2 acts as an inner filter at λ = 248 nm in the used measurement cell and reduce the number of photons of the ferricyanide photolysis. In Table SI 1 the calculated concentrations of the photolysis fragments considering the absorption of H_2O_2 are shown. These calculations were done by using the average laser pulse energy in the measurement cell of E = 177 mJ. The resulting concentration of the transient species corresponds to about 7% compared to the formed OH radical concentration. It is assumed that the species $K_3[Fe(CN)_5(H_2O)]$ produced from the photo induced ligand exchange will react with the formed alkyl radicals in the same way as $K_3[Fe(CN)_6]$.

$$K_3[Fe(CN)_6] + h\nu\ (\lambda = 248\ nm) \longrightarrow K_3[Fe(CN)_5(H_2O)] + CN^- \qquad (R\text{-}1)$$

$$HCN^- + \cdot OH \longrightarrow \cdot C(OH)=N^- \qquad (R\text{-}2)$$

$$\cdot C(OH)=N^- + \cdot C(OH)=N^- \longrightarrow \text{Products} \qquad (R\text{-}3)$$

The formed cyanide (R-1) is fully protonated under this experimental conditions ($pK_a = 9.31$) and will react by OH radical addition (R-2).[6] The formed product undergoes a recombination reaction (R-3). Overall, the photo induced ligand exchange leads to a decrease of the alkyl radical concentration, due to the consumption of OH radicals as well as the consumption by OH-adduct radical $\cdot C(OH)=N^-$.

Table SI 1: Change of the initial concentration of OH radicals and the photolysis fragments concentration of the ferricyanide complex with $[H_2O_2] = 5 \times 10^{-3}$ M and [Reactant] $= 1 \times 10^{-3}$ M

$K_3[Fe(CN)_6]$ M	$[OH]_0$ M	Photolysis fragment of $K_3[Fe(CN)_6]$			
		$K_3[Fe(CN)_5(H_2O)]$ M		(CN^-) M	
		$\Phi = 0.02$	$\Phi = 0.04$	$\Phi = 0.02$	$\Phi = 0.04$
1×10^{-5}	8.22×10^{-6}	1.07×10^{-8}	2.14×10^{-8}	1.07×10^{-8}	2.14×10^{-8}
3×10^{-5}	7.81×10^{-6}	3.21×10^{-8}	6.42×10^{-8}	3.21×10^{-8}	6.42×10^{-8}
5×10^{-5}	7.42×10^{-6}	5.35×10^{-8}	1.07×10^{-7}	5.35×10^{-8}	1.07×10^{-7}
7×10^{-5}	7.06×10^{-6}	7.49×10^{-8}	1.50×10^{-7}	7.49×10^{-8}	1.50×10^{-7}
9×10^{-5}	6.73×10^{-6}	9.62×10^{-8}	1.92×10^{-7}	9.62×10^{-8}	1.92×10^{-7}

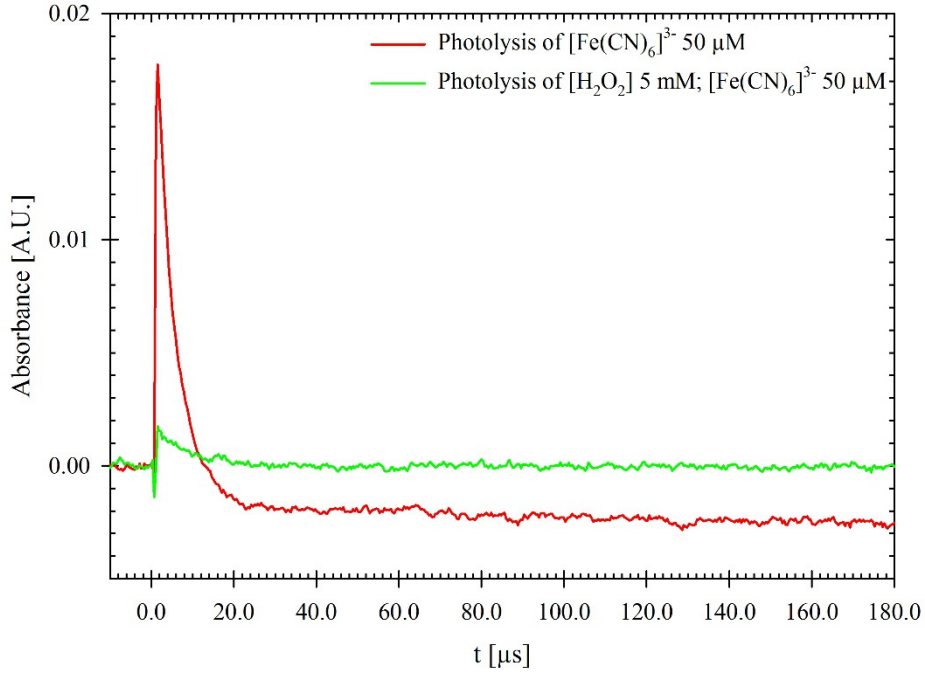

Figure SI 12: Measured absorption - time profiles at λ = 442 nm of the photolysis of [$K_3[Fe(CN)_6]$] = 5 × 10^{-5} M (red) and [$K_3[Fe(CN)_6]$] = 5 × 10^{-5} M with [H_2O_2] = 5 × 10^{-3} M (green).

Investigation of the reaction of ferrocyanide with H_2O_2

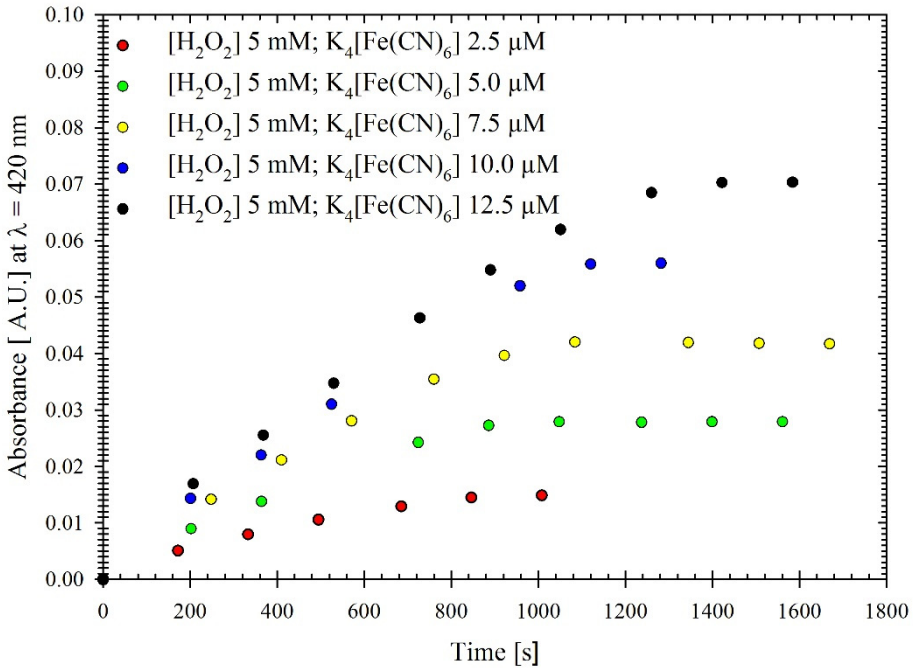

Figure SI 13: Measured absorption - time profiles at λ = 420 nm of the oxidation reaction of ferrocyanide with H_2O_2 at pH = 2 to form the absorbing ferricyanide.

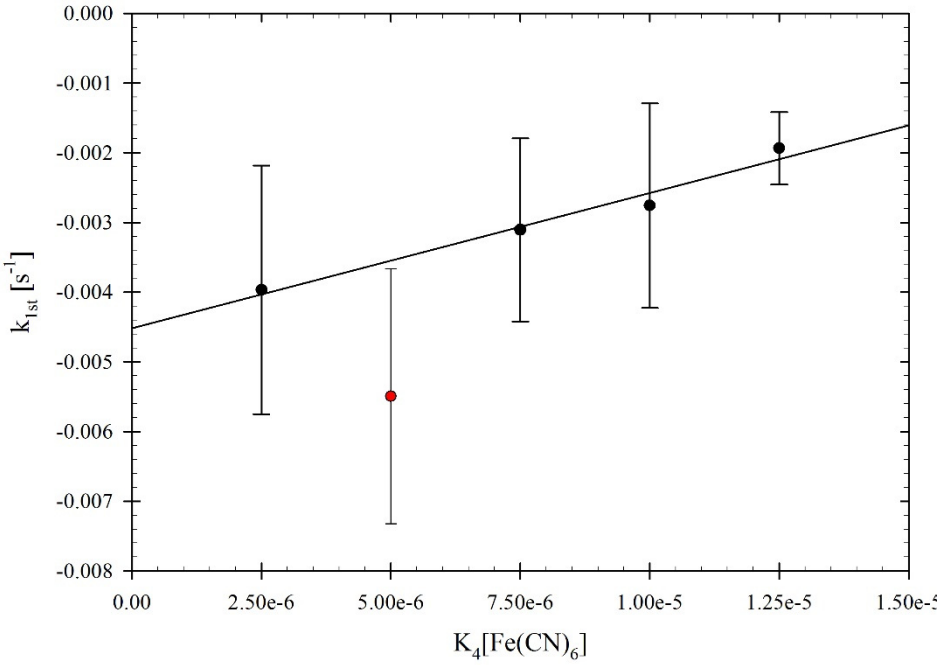

Figure SI 14: The averaged first-order rate constants of the decay of ferrocyanide with H_2O_2 at pH = 2 plotted against the ferrocyanide concentrations.

The build-up of the absorption at λ = 420 nm of ferricyanide in the reaction of H_2O_2 with ferrocyanide is shown in Figure SI 13. The averaged first-order rate constants derived from the curves in Figure SI 13 are linear with ferrocyanide concentration (Figure SI 14). From the slope of the plot, the bimolecular rate constant for the reaction of ferrocyanide with H_2O_2 was k = 194 ± 103 l mol^{-1} s^{-1}. The k_{1st} rate constant at the ferrocyanide concentration 5 × 10^{-6} M was not considered for the slope calculations (Figure SI 14). This reaction rate explains the similar absorption behaviour in Figure SI 4, SI 9 and SI 16. The contribution of the formed HO_2 and O_2^- radicals for the oxidation of ferrocyanide is too small to explain this absorption behaviour.

Glyoxal:

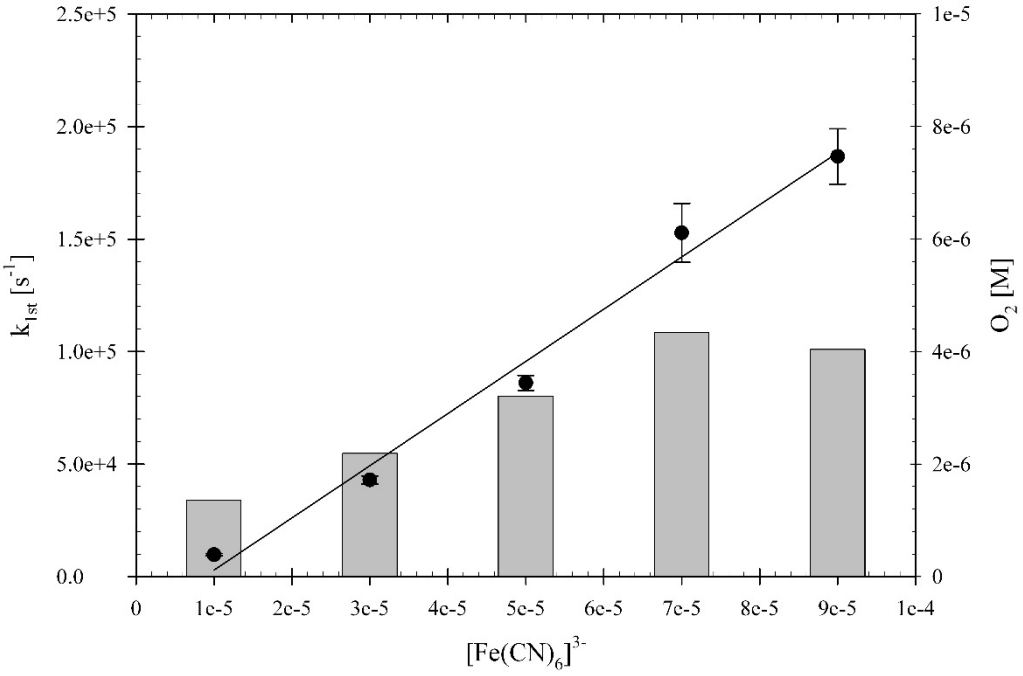

Figure SI 15: The averaged first-order rate constants of the reaction with the glyoxyl alkyl radical (left axis) for five different ferricyanide concentrations plotted against these concentrations. At the right axis the measured oxygen concentration is given.

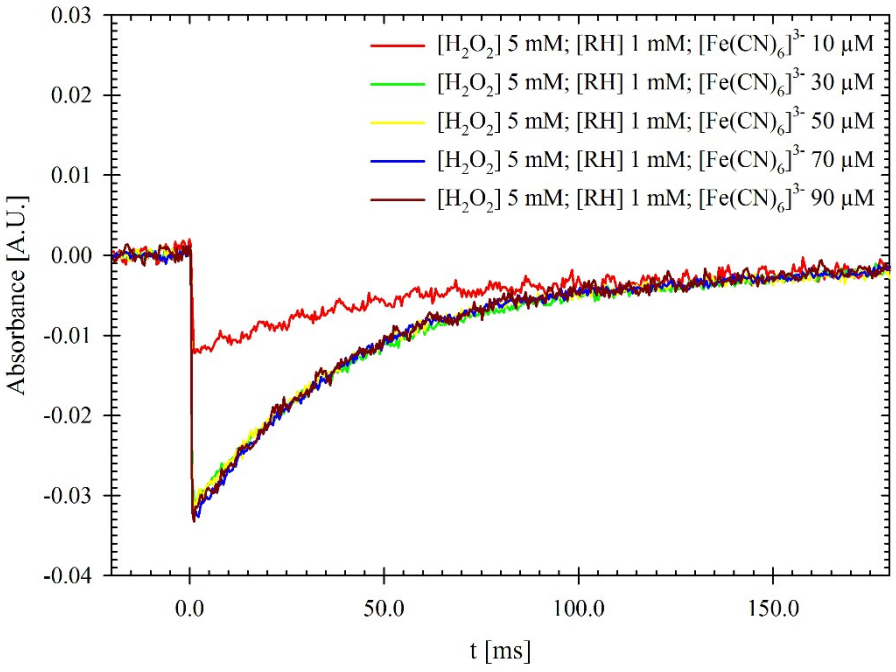

Figure SI 16: Measured absorption - time profiles at λ = 442 nm of the reaction from the formed ferrocyanide with H_2O_2 in the investigation of the glyoxal oxidation.

Model reaction mechanism

The COPASI model mechanism (Table SI 2) includes a fixed OH concentration, the HO_x side reactions, the H atom abstraction reaction and the organic radical reactions. This model mechanism was based on Schaefer et al..[7] The transient species were formed in the oxidation of 1×10^{-3} M glyoxal with OH radicals at pH = 2 in oxygen saturated solution $[O_2] = 1.00 \times 10^{-3}$ M. The latter were generated by photolysis of 2×10^{-4} M H_2O_2 at $\lambda = 248$ nm. The OH radical concentration $[OH]_0 = 6.41 \times 10^{-7}$ M was determined by the direct observation of the OH radical at $\lambda = 244$ nm by using the same conditions without the organic reactant, the molar absorption coefficient $\varepsilon(OH) = 530$ M^{-1} cm^{-1} after Herrmann et al. and the molar absorption coefficient $\varepsilon(HO_2) = 961$ M^{-1} cm^{-1} after Behar et al..[5, 8]

Table SI 2: Full reaction mechanism with rate constants used to simulate the experiments with $[H_2O_2] = 2 \times 10^{-4}$ M and [Glyoxal] = 1×10^{-3} M at pH = 2.

	Reactions	Parameter	Comment
	Equilibria	pKa	
R-1	$H_2O \rightleftharpoons H^+ + OH^-$	13.999	9
R-2	$HO_2 \rightleftharpoons O_2^- + H^+$	4.57	9
	Acid - Base Reactions		
R-3	$H^+ + OH^- \longrightarrow H_2O$	1.4×10^{11} M^{-1} s^{-1}	9
R-4	$H_2O \longrightarrow H^+ + OH^-$	$k_3 \times K_1 / [H_2O]$	9
R-5	$HO_2 \longrightarrow O_2^- + H^+$	$k_6 \times K_2$	9
R-6	$O_2^- + H^+ \longrightarrow HO_2$	5×10^{10} M^{-1} s^{-1}	9
R-7	$HO_2 + OH^- \longrightarrow O_2^- + H_2O$	5×10^{10} M^{-1} s^{-1}	9
R-8	$O_2^- + H_2O \longrightarrow HO_2 + OH^-$	$k_7 \times K_1 / K_2 \times [H_2O]$	9
	Chemical Reactions		
R-9	$H_2O_2 + h\nu \longrightarrow 2\ OH$	$\Phi = 1$	5
R-10	$2\ OH \longrightarrow H_2O_2$	5.5×10^9 M^{-1} s^{-1}	10
R-11	$OH + H_2O_2 \longrightarrow H_2O + HO_2$	3.0×10^7 M^{-1} s^{-1}	11
R-12	$OH + HO_2 \longrightarrow H_2O + O_2$	6.0×10^9 M^{-1} s^{-1}	12
R-13	$OH + O_2^- \longrightarrow OH^- + O_2$	1.1×10^{10} M^{-1} s^{-1}	13
R-14	$2\ HO_2 \longrightarrow H_2O_2 + O_2$	9.8×10^5 M^{-1} s^{-1}	14
R-15	$HO_2 + H_2O_2 \longrightarrow OH + O_2 + H_2O$	5×10^{-1} M^{-1} s^{-1}	9
R-16	$2\ O_2^- + 2\ H_2O \longrightarrow H_2O_2 + O_2 + 2\ OH^-$	$1 \times 10_2$ s^{-1}/ $[H_2O]$	14

R-17	$HO_2 + O_2^- \longrightarrow HO_2^- + O_2$	8.4×10^7 M^{-1} s^{-1}	14
R-18	$CH(OH)_2CH(OH)_2 + OH \longrightarrow C(OH)_2CH(OH)_2$	9.2×10^8 M^{-1} s^{-1}	this work
R-19	$C(OH)_2CH(OH)_2 + O_2 \longrightarrow CH(OH)_2C(OH)_2O_2$	1.2×10^9 M^{-1} s^{-1}	fitted
R-20	2 C(OH)2CH(OH)2 $\longrightarrow$ Product 1	1.0×10^9 M^{-1} s^{-1}	estimated
R-21	$C(OH)_2CH(OH)_2 + H_2O_2 \longrightarrow$ Product 2	2×10^5 M^{-1} s^{-1}	estimated
R-22	$CH(OH)_2C(OH)_2O_2 + HO_2 \longrightarrow$ Product 3	1.0×10^8 M^{-1} s^{-1}	estimated
R-23	$CH(OH)_2C(OH)_2O_2 + O_2^- \longrightarrow$ Product 4	1.0×10^9 M^{-1} s^{-1}	estimated
R-24	$CH(OH)_2C(OH)_2O_2 + H_2O_2 \longrightarrow$ Product 5	1.0×10^4 M^{-1} s^{-1}	estimated
R-25	$CH(OH)_2C(OH)_2O_2 \longrightarrow HO_2 + CH(OH)_2C(O)OH$	155 s^{-1}	fitted
R-26	2 $CH(OH)_2C(OH)_2O_2 \longrightarrow$ 2 $CH(OH)_2C(OH)_2O$	9.4×10^7 M^{-1} s^{-1}	fitted
R-27	$CH(OH)2C(OH)2 \longrightarrow CH(OH)C(O)OH + H_2O$	2.7×10^5 s^{-1}	derived from Fig. SI 17
R-28	$CH(OH)C(O)OH + O_2 \longrightarrow O_2CH(OH)C(O)OH$	1.8×10^9 M^{-1} s^{-1}	2
R-29	2 CH(OH)C(O)OH $\longrightarrow$ Product 6	5.5×10^8 M^{-1} s^{-1}	15
R-30	$O_2CH(OH)C(O)OH \longrightarrow HO_2 + CH(O)C(O)OH$	200 s^{-1}	estimated
R-31	$CH(OH)C(O)OH + H_2O_2 \longrightarrow$ Product 7	2×10^5 M^{-1} s^{-1}	estimated
R-32	$O_2CH(OH)C(O)OH + H_2O_2 \longrightarrow$ Product 8	1.0×10^4 M^{-1} s^{-1}	estimated
R-33	$O_2CH(OH)C(O)OH + HO_2 \longrightarrow$ Product 9	1.0×10^8 M^{-1} s^{-1}	estimated
R-34	$O_2CH(OH)C(O)OH + CH(OH)_2C(OH)_2O_2 \longrightarrow$ Product 10	1.0×10^8 M^{-1} s^{-1}	estimated

The estimation of the rate constants in Table SI 2 was based on literatur values for the kind of reactions under consideration. In the case of the alkyl radical recombination reaction R-20 the rate constant of the recombination 1-hydroxyethyl alkyl radical ($k = 1 \times 10^9$ M^{-1} s^{-1}) was taken from Seddon and Allen.[16] The rate constant of the H atom abstraction reaction from hydrogen peroxid by the alkyl radicals (R-21 and R-31) as upper limit was based on the rate constants ($k = 1.5 \times 10^5$ - 2.8×10^5 M^{-1} s^{-1}) obtained from reaction of an 1-hydroxyethyl alkyl radical with hydrogen peroxide.[16-19] The decrease of this rate constant by two orders of magnitude shows no influence on the fitted rate constants (R-19, R-25, R-26), due to the oxygen addition reaction R-19 and the dehydration reaction (R-27). The reaction (R-22, R-33 and R-34) was estimated, using the typical order of magnitude for peroxyl radical recombination reactions $k \approx 10^8$ M^{-1} s^{-1}.[20, 21] Bothe et al. reported a estimated rate constant for the reaction of HO_2 radicals with the 1-hydroxyethyl peroxyl radical with $k = 10^7$ M^{-1} s^{-1}.[22] A drecrease of the rate constant (R-22) to $k = 10^7$ $M^{-1}s^{-1}$ would result in poorer model fit, because of the poor description of the

HO_2 radical. This would also lead to a decrease of the fitted rate constant of the HO_2 elimination reaction (R-25) with $k_{1st} < 12\ s^{-1}$. In comparison to the literature values given in Alfassi (k_{1st} = 50 -700 s^{-1}) the resulting value appear too low.[20] Due to this, the rate constant (R-22) was set to $k = 1 \times 10^8\ M^{-1}\ s^{-1}$. It is known that $O_2^{\cdot -}$ radical anion react with peroxyl radicals by electron transfer with a rate constant $k = 10^9\ M^{-1}\ s^{-1}$, yielding the corresponding hydroperoxide.[23] Under the used conditions (pH =2) the $O_2^{\cdot -}$ radical anion is fully protonated and this reaction (R-23) is negligible. The H atom abstraction reaction rate constant from hydrogen peroxide by peroxyl radicals (R-24 and R-32) was also used as an upper limit, as in the reaction (R-21 and R-31). The variation to a smaller value $k = 100\ M^{-1}\ s^{-1}$) shows also no influence. The rate constant of the acid-catalyzed dehydration reaction (R-27) was derived from the linear slope shown in the inset of Figure SI 17 (Page 19) under reduced oxygen concentration. The rate constant k = 200 s^{-1} of the HO_2 radical elimination reaction (R-30) was based on rate constants given in Alfassi for 1,2-dihydroxyethyl alkyl radicals with k(HO_2 elimination) = 190 s^{-1}.[20]

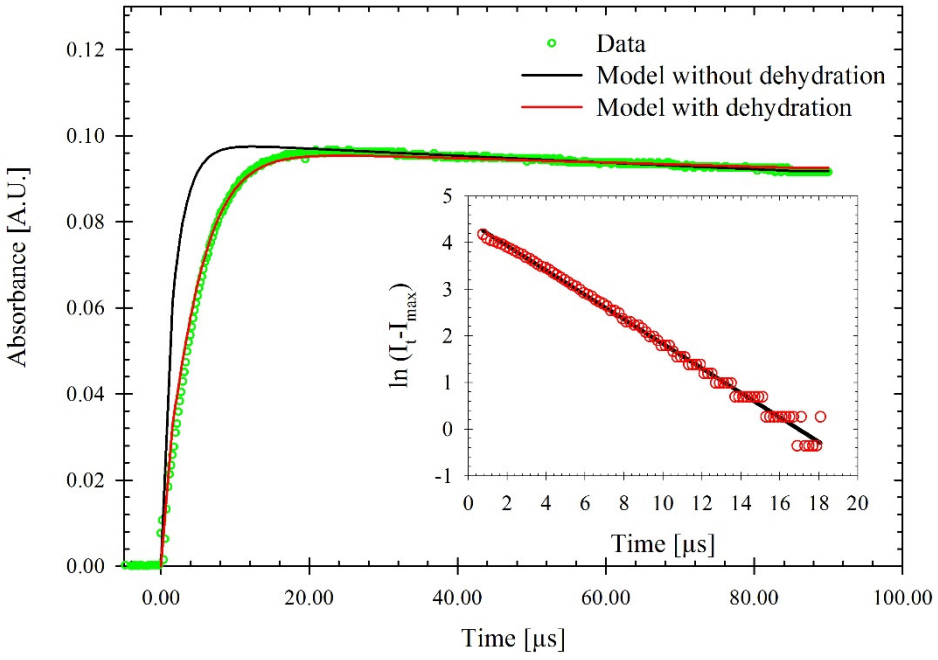

Figure SI 17: Measured - time profiles at λ = 244 nm of the glyoxal oxidation in oxygen reduced solution. The modelling provided the first order rate constant of the acid-catalyzed dehydration reaction.

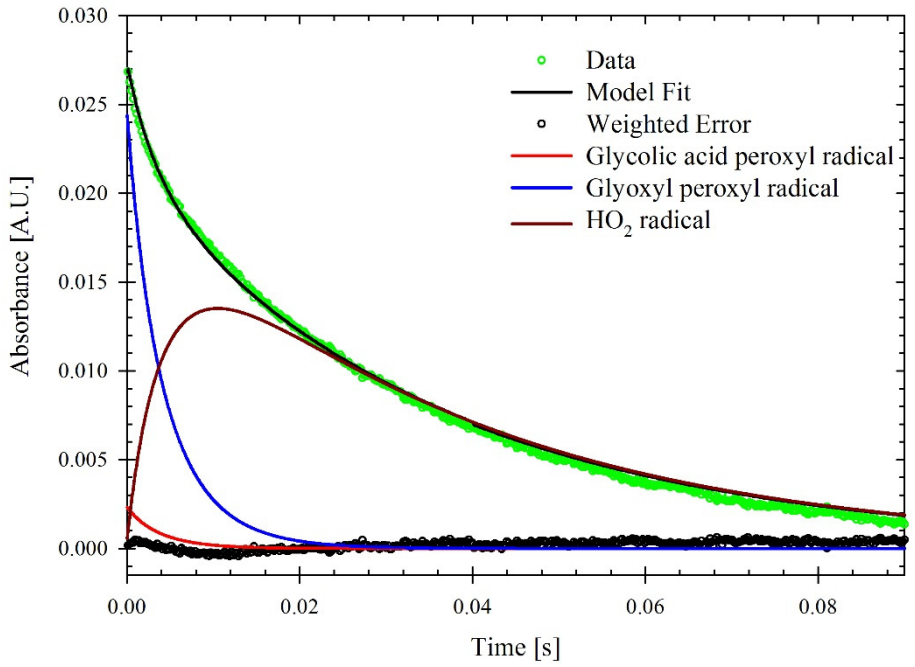

Figure SI 18: Measured and modelled absorption - time profiles at λ = 244 nm of the decay of HO_2, glyoxyl peroxyl and glycolic acid peroxyl radical in an oxygen saturated solution.

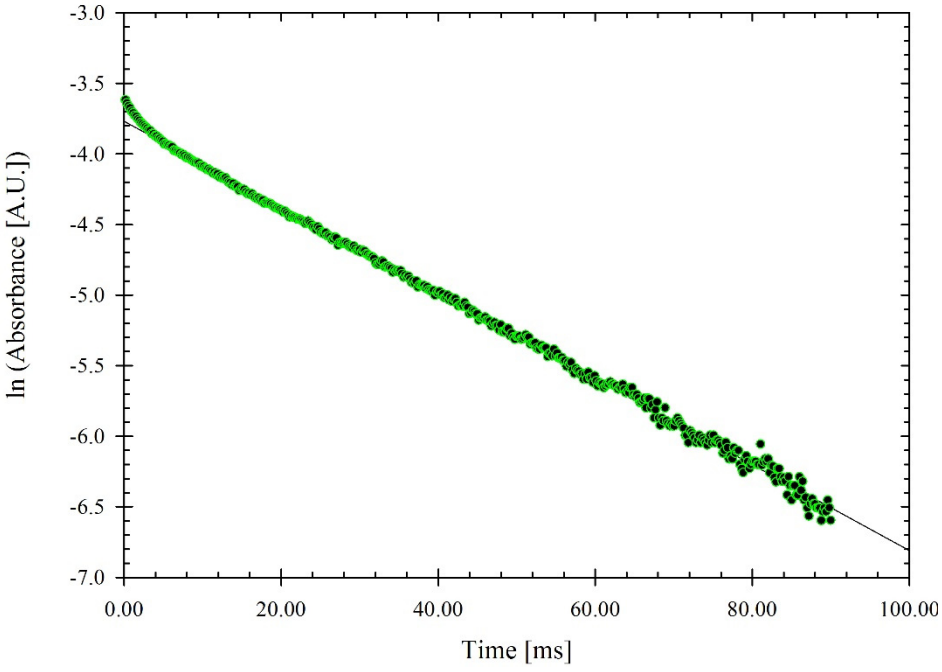

Figure SI 19: Classical method ln c vs. t for the determination of k_{1st} derived from absorption - time profiles at λ = 244 nm of an oxygen saturated solution.

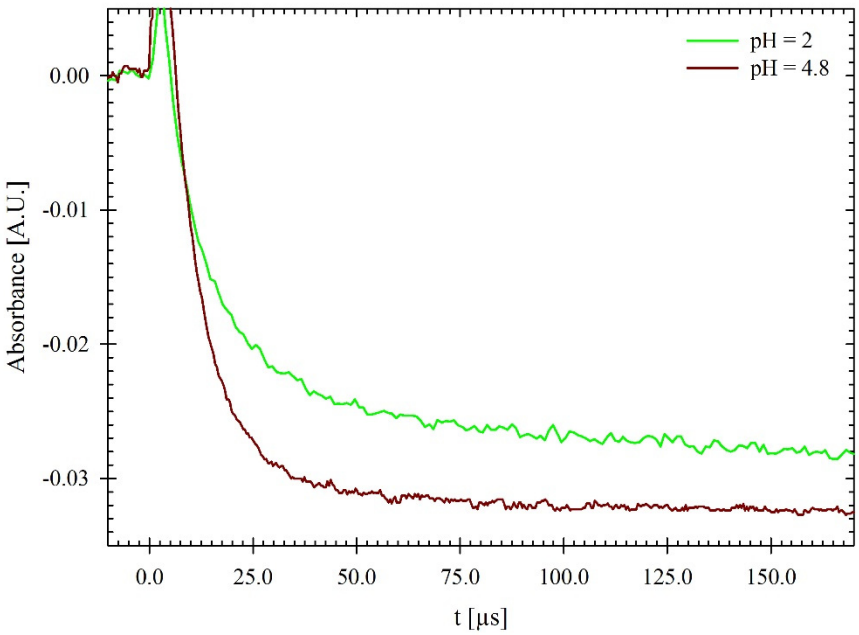

Figure SI 20: Absorbance change for the different solutions, with the concentrations with $[H_2O_2] = 5 \times 10^{-3}$ M, [Glyoxal] = 1×10^{-3} M, $[K_3[Fe(CN)_6]] = 5 \times 10^{-5}$ M and at various pH values.

Table SI 3: Influence of the change of the molar absorption coefficient of the glycolic acid alkyl ε(R') and peroxyl radical ε(R'O_2) on the oxygen addition reaction of glyoxyl alkyl radical ε(R) to the glyoxyl peroxyl radical ε(RO_2) at λ = 244nm.

Model case	ε(R') l mol^{-1} cm^{-1}	ε(R'O_2) l mol^{-1} cm^{-1}	ε(R) l mol^{-1} cm^{-1}	ε(RO_2) l mol^{-1} cm^{-1}	k(R + O_2) l mol^{-1} s^{-1}
I	0	0	1265	1127	8.4×10^8
II	3250	0	1073	1031	1.5×10^9
III	3250	250	1066	1003	1.3×10^9
IV	3250	500	1060	969	1.2×10^9
V	3250	500	803	1299	2.0×10^8 *
VI	3250	500	2201	917	5.0×10^9 *
VII	3250	750	1076	924	1.2×10^9
VIII	3250	1000	1092	875	1.1×10^9

* fixed rate constant

Product analysis. The measurement cell as described before was also used for the product studies. A solution containing 5×10^{-3} M H_2O_2 and 1×10^{-3} M glyoxal at pH = 4.8 was irradiated with a series of laser pulses at λ = 248 nm. After the pulses an aliquot of the solution was taken off the cell and H_2O_2 was destroyed by adding a sufficient concentration of catalase.[24] The formed carboxylic acids were analysed by an capillary electrophoresis method after Scheinhardt et al..[25] In brief, a background electrolyte consisting of 2 mM 5- sulfosalicylic acid, 8 mM tris(hydroxyl-methyl)aminomethane and 0.001% hexadimethrine bromide at a pH of 8.2 was used in an Agilent 7100 capillary electrophoresis system. An uncoated fused-silica capillary with an inner diameter of 75 μm and a total length of 80.5 cm (72 cm to the detector) was used.

Influence of triplet state glyoxylic acid

The deprotonated form of glyoxylic acid (pKa = 3.2) is the dominant form with 97.6% under the used conditions (pH = 4.8).[26] A hydration constant can be found in Tyr'yan, with K_{Hyd} = 67.[27] The resulting concentration fraction of the dehydrated glyoxalate is smaller than 2%. Also, Leitzke et al. calculated a similar fraction of 1.8% from NMR data.[28] However, glyoxylic acid is produced with a concentration of (c(glyoxylic acid) ≈ 7×10^{-6} M) per pulse. The resulting concentration of the dehydrated glyoxalate can be given with 1.4×10^{-7} M. The impurities in the beginning of the experiments (0 Pulses Start) deliver a concentration of 2×10^{-6} M of glyoxylic acid, whereas the dehydrated form has a concentration of 4×10^{-8} M. Under reduced oxygen conditions, the formed triplet state could react either with hydrated glyoxylic acid or with hydrogen peroxide. Porter et al. described the H atom abstraction mechanism of a triplet state carbonyl compound for acetone.[29] The reaction with H_2O_2 forms the glycolic acid alkyl radical and a HO_2 radical. The reaction of the triplet state of dehydrated glyoxylic acid with another glyoxylic acid molecule leads also to the glycolic acid alkyl radical and to a hydrated formyl radical. These formed radicals and the glyoxyl alkyl radical from the OH radical

oxidation reaction could undergo a recombination reaction. The formed product might also explain the unknown product in the product studies. It has to be mentioned that under tropospheric conditions the triplet state is expected to be quenched by molecular oxygen.

Investigations of the OH, SO_4^- and NO_3 radical reactivity.

The reactivity of OH, SO_4^- or NO_3 radicals with glyoxal in aqueous solution was determined using a thermostated laser flash photolysis - laser long - path absorption (LP-LLPA) setup, which is described in more detail.[7] All kinetic experiments were carried out under first order conditions adding glyoxal in excess to the formed radical with the following glyoxal concentrations 0 M, 5×10^{-5} M, 1×10^{-4} M, 1.5×10^{-4} M, 2×10^{-4} M. The measurements of the kinetics of OH and SO_4^- radicals were done in a high-purity silica cell of 147 cm³ volume with a photolysis path length of 7 cm. The White cell mirror configuration was adjusted for 8 passes giving an absorption path length of 56 cm at the wavelength $\lambda = 407$ nm to measure the temporal change of the radical concentration by cw-laser (Coherent, 0222-583-00). The reactivity of the OH radical reaction was determined by the competition kinetic method by using the photolysis of hydrogen peroxide (H_2O_2; 2×10^{-4} M) at $\lambda = 248$ nm and thiocyanate (KSCN; 2×10^{-5} M) as reference system. [30] The rate constant of the reaction of glyoxal with sulphate radicals (SO_4^-), which were formed by the photolysis of peroxodisulfate ($K_2S_2O_8$; 5×10^{-4} M) at $\lambda = 248$ nm, was measured by direct observation at $\lambda = 407$ nm. The investigations of the reactivity of the nitrate radical (NO_3) were done in a high-purity silica cell of 7.1 cm³ volume with a photolysis path length of 6.3 cm. Due to a mirror configuration with 3 passes leads to an absorption path length of 19 cm. The nitrate radicals were formed from the photolysis of $K_2S_2O_8$ (0.03 M) in the presence of potassium nitrate ($NaNO_3$; 0.1 M) at $\lambda = 351$ nm. The changes of the nitrate radical concentration were measured directly using a continuous wave semiconductor laser at the wavelength $\lambda = 635$ nm.

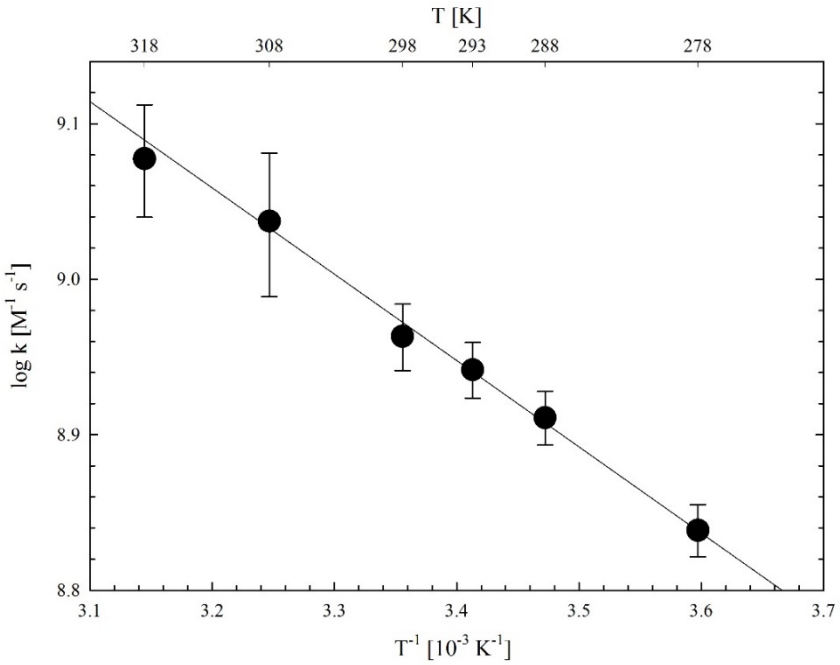

Figure SI 21: Arrhenius plot for the reaction of OH radicals with glyoxal in aqueous solution.

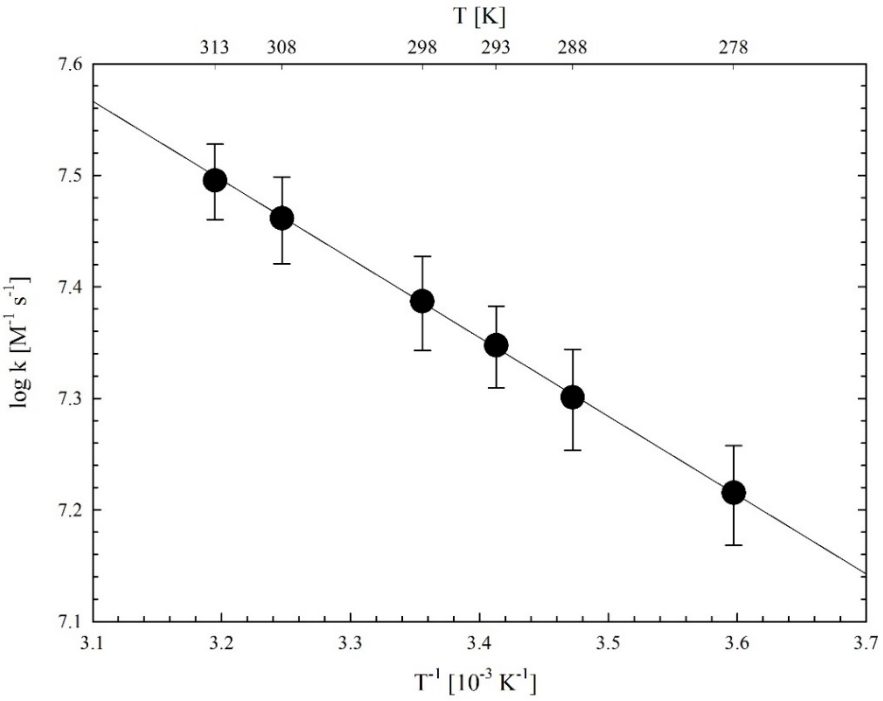

Figure SI 22: Arrhenius plot for the reaction of sulphate radicals with glyoxal in aqueous solution.

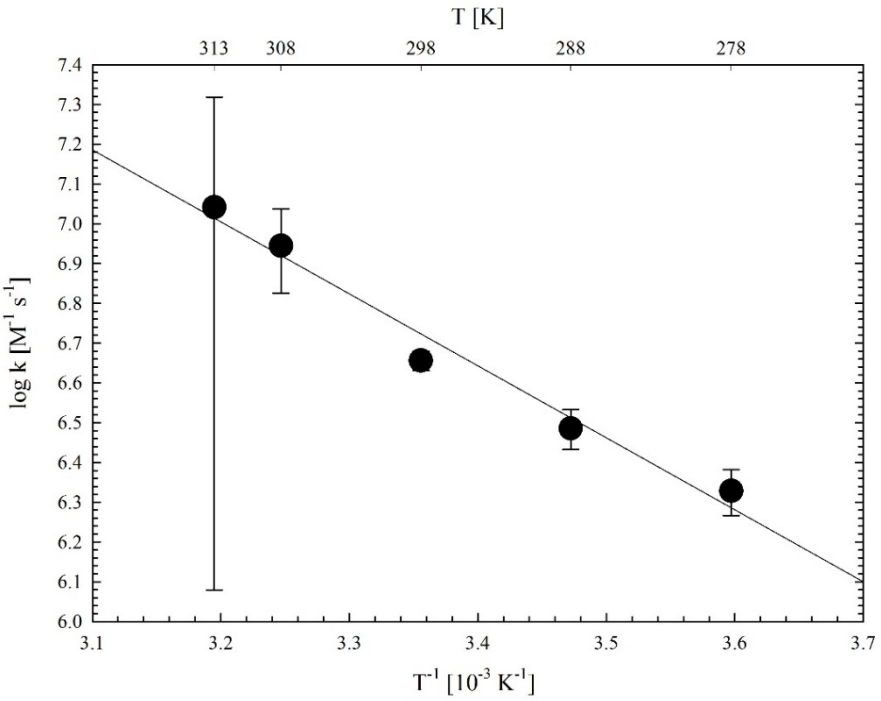

Figure SI 23: Arrhenius plot for the reaction of nitrate radicals with glyoxal in aqueous solution.

Table SI 4: Temperature dependent second-order rate constants for the OH, SO_4^- and NO_3 radical reaction with glyoxal.

Temperature [K]	OH rate constant [M^{-1} s^{-1}]	SO_4^- rate constant [M^{-1} s^{-1}]	NO_3 rate constant [M^{-1} s^{-1}]
278	$(6.9 \pm 0.3)\times10^8$	$(1.6 \pm 0.2)\times10^7$	$(2.1 \pm 0.3)\times10^6$
288	$(8.2 \pm 0.3)\times10^8$	$(2.0 \pm 0.2)\times10^7$	$(3.1 \pm 0.4)\times10^6$
293	$(8.7 \pm 0.4)\times10^8$	$(2.2 \pm 0.2)\times10^7$	/
298	$(9.2 \pm 0.5)\times10^8$	$(2.4 \pm 0.2)\times10^7$	$(4.5 \pm 0.3)\times10^6$
308	$(1.1 \pm 0.1)\times10^9$	$(2.9 \pm 0.3)\times10^7$	$(8.8 \pm 2.1)\times10^6$
313	/	$(3.1 \pm 0.2)\times10^7$	$(1.1 \pm 1.0)\times10^7$
318	$(1.2 \pm 0.1)\times10^9$	/	/

References for the Supporting Information

1. Fuller, M. W.; Lebrocq, K. M. F.; Leslie, E.; Wilson, I. R., The Photolysis of aqueous-solutions of potassium hexacyanoferrate (III). *Austr. J. Chem.* **1986,** *39*, (9), 1411-1419 DOI: 10.1071/CH9861411.
2. Adams, G. E.; Willson, R. L., Pulse radiolysis studies on the oxidation of organic radicals in aqueous solution. *Trans. Faraday Soc.* **1969,** *65*, 2981-2987 DOI: 10.1039/TF9696502981.
3. Pilling, M. J.; Seakins, P. W., *Reaction Kinetics*. Oxford Science Publications: Oxford, New York, Tokyo, 1995.
4. Herrmann, H., On the photolysis of simple anions and neutral molecules as sources of O^- /OH, SO_x^- and Cl in aqueous solution. *Phys. Chem. Chem. Phys.* **2007,** *9*, (30), 3935-3964 DOI: 10.1039/B618565g.
5. Herrmann, H.; Hoffmann, D.; Schaefer, T.; Bräuer, P.; Tilgner, A., Tropospheric aqueous-phase free-radical chemistry: Radical sources, spectra, reaction kinetics and prediction tools. *ChemPhysChem* **2010,** *11*, (18), 3796-3822 DOI: 10.1002/cphc.201000533.
6. Büchler, H.; Bühler, R. E.; Cooper, R., Pulse radiolysis of aqueous cyanide solutions. Kinetics of the transient hydroxyl radical and hydrogen atom adducts and subsequent rearrangements. *J. Phys. Chem.* **1976,** *80*, (14), 1549-1553 DOI: 10.1021/j100555a006.
7. Schaefer, T.; Schindelka, J.; Hoffmann, D.; Herrmann, H., Laboratory kinetic and mechanistic studies on the OH-initiated oxidation of acetone in aqueous solution. *J. Phys. Chem. A* **2012,** *116*, (24), 6317-6326 DOI: 10.1021/jp2120753.
8. Behar, D.; Czapski, G.; Rabani, J.; Dorfman, L. M.; Schwarz, H. A., Acid dissociation constant and decay kinetics of the perhydroxyl radical. *J. Phys. Chem.* **1970,** *74*, (17), 3209-3213 DOI: 10.1021/j100711a009.
9. Pastina, B.; LaVerne, J. A., Effect of molecular hydrogen on hydrogen peroxide in water radiolysis. *J. Phys. Chem. A* **2001,** *105*, (40), 9316-9322 DOI: 10.1021/jp012245j.
10. Buxton, G. V.; Greenstock, C. L.; Helman, W. P.; Ross, A. B., Critical review of rate constants for reactions of hydrated electrons, hydrogen atoms and hydroxyl radicals (OH/O^-) in aqueous solution. *J. Phys. Chem. Ref. Data* **1988,** *17*, 513-886; 10.1063/1.555805.
11. Christensen, H.; Sehested, K.; Corfitzen, H., Reactions of hydroxyl radicals with hydrogen peroxide at ambient and elevated temperatures. *J. Phys. Chem.* **1982,** *86*, 1588-1590 DOI: 10.1021/j100206a023.
12. Elliot, A. J.; Buxton, G. V., Temperature dependence of the reactions OH+ O_2^- and OH + HO_2 in water up to 200°C. *J. Chem. Soc. Faraday Trans.* **1992,** *88*, (17), 2465-2470 DOI: 10.1039/FT9928802465.
13. Christensen, H.; Sehested, K.; Bjergbakke, E., Radiolysis of reactor water: Reaction of hydroxyl radicals with superoxide (O_2^-). *Water Chemistry Of Nuclear Reactor Systems* **1989,** *5*, 141-144 DOI: 10.1680/wconrs5v1.15470.
14. Christensen, H.; Sehested, K., HO_2 and O_2^- radicals at elevated temperatures. *J. Phys. Chem.* **1988,** *92*, 3007-3011 DOI: 10.1021/j100321a060.
15. Simic, M.; Neta, P.; Hayon, E., Pulse radiolysis of aliphatic acids in aqueous solutions. II. Hydroxy and polycarboxylic acids. *J. Phys. Chem.* **1969,** *73*, (12), 4214-4219 DOI: 10.1021/j100846a030.
16. Seddon, W. A.; Allen, A. O., Radiation chemistry of aqueous solutions of ethanol. *J. Phys. Chem.* **1967,** *71*, (6), 1914-1918 DOI: 10.1021/j100865a059.

17. Gilbert, B. C.; Jeff, M., Free Radicals: Chemistry, Pathology and Medicine. In *Free Radicals: Chemistry, Pathology and Medicine*, Evans, C. R.; Dormandy, T., Eds. Richelieu Press: London, England, 1988; pp 25-49.
18. Kishore, K.; Moorthy, P.; Rao, K., Reactivity of H_2O_2 with radiation produced free radicals: Steady state radiolysis methods for estimating the rate constants. *Int. J. Radiat. Appl. Instrum. C Radiat. Phys. Chem.* **1987,** *29*, (4), 309-313 DOI: 10.1016/1359-0197(87)90037-3.
19. NIST Solution Kinetics Database Version 3.0, NIST, Gaithersburg, 1998.
20. Alfassi, Z. B., *The Chemistry of Free Radicals: Peroxyl Radicals*. John Wiley & Sons: West Sussex, England, 1997.
21. Neta, P.; Grodkowski, J.; Ross, A. B., Rate constants for reactions of aliphatic carbon‐centered radicals in aqueous solution. *J. Phys. Chem. Ref. Data* **1996,** *25*, (3), 709-1050 DOI: 10.1063/1.555978.
22. Bothe, E.; Schuchmann, M. N.; Schulte-Frohlinde, D.; von Sonntag, C., Hydroxyl radical-induced oxidation of ethanol in oxygenated aqueous solutions. A pulse radiolysis and product study. *Z. Naturforsch.* **1983,** *38B*, 212-219.
23. Schuchmann, M. N.; Von Sonntag, C., The rapid hydration of the acetyl radical. A pulse radiolysis study of acetaldehyde in aqueous solution. *J. Am. Chem. Soc.* **1988,** *110*, (17), 5698-5701 DOI: 10.1021/ja00225a019.
24. Ogura, Y., Catalase activity at high concentration of hydrogen peroxide. *Arch. Biochem. Biophys.* **1955,** *57*, (2), 288-300 DOI: 10.1016/0003-9861(55)90291-5.
25. Scheinhardt, S.; Müller, K.; Spindler, G.; Herrmann, H., Complexation of trace metals in size-segregated aerosol particles at nine sites in Germany. *Atmos. Environ.* **2013,** *74*, 102–109 DOI: 10.1016/j.atmosenv.2013.03.023.
26. Hoigné, J.; Bader, H., Rate constants of reactions of ozone with organic and inorganic compounds in water—II: dissociating organic compounds. *Water Res.* **1983,** *17*, (2), 185-194 DOI: 10.1016/0043-1354(83)90099-4.
27. Tur'yan, Y. I., Kinetics and equilibrium of the dehydration-hydration and recombination-dissociation reactions of glyoxylic acid investigated by electrochemical methods. *Croat. Chem. Acta* **1998,** *71*, 727-743.
28. Leitzke, A.; Reisz, E.; Flyunt, R.; von Sonntag, C., The reactions of ozone with cinnamic acids: formation and decay of 2-hydroperoxy-2-hydroxyacetic acid. *J. Chem. Soc., Perkin Trans. 2* **2001**, (5), 793-797 DOI: 10.1039/B009327K.
29. Porter, G.; Dogra, S.; Loutfy, R.; Sugamori, S.; Yip, R., Triplet state of acetone in solution. Deactivation and hydrogen abstraction. *J. Chem. Soc., Faraday Trans. 1* **1973,** *69*, 1462-1474 DOI: 10.1039/F19736901462.
30. Zhu, L.; Nicovich, J. M.; Wine, P. H., Temperature-dependent kinetics studies of aqueous phase reactions of hydroxyl radicals with dimethylsulfoxide, dimethylsulfone, and methanesulfonate. *Aquat. Sci.* **2003,** *65*, (4), 425-435 DOI: 10.1007/s00027-003-0673-6.